23rd International Conference on Renewable Energies and Power Quality (ICREPQ'25)
Tenerife (Spain), 25th to 27th June 2025
Renewable Energy and Power Quality Journal (RE&PQJ)
ISSN 2172-038 X, Volume No.23, September 2025

Adaptive PI state control of a two-mass oscillator system for active damping of torsional vibrations in deep drilling technology

Daniel Alexander Piontek[1], Alexander Oberland[2], Hans-Peter Beck[3], Dirk Turschner[4] and Ines Hauer[5]

[1345] Institute of Electrical Power Engineering and Energy Systems, [2] Clausthal Centre of Material Technology
Clausthal University of Technology
Leibnizstraße 28, 38678 Clausthal-Zellerfeld (Germany)

[1] Phone number: +49-5323-72-3728, e-mail: daniel.alexander.piontek@tu-clausthal.de
[2] Phone number: +49-5321-3816-8071, e-mail: alexander.oberland@tu-clausthal.de
[3] Phone number: +49-5321-3816-8001, e-mail: hans-peter.beck@tu-clausthal.de
[4] Phone number: +49-5323-72-2592, e-mail: turschner@iee.tu-clausthal.de
[5] Phone number: +49-5323-72-2176, e-mail: ines.hauer@tu-clausthal.de

Abstract. Torsional vibrations in deep drilling systems, such as the nonlinear stick-slip effect, pose significant challenges to operational stability and tool longevity. Building on previously derived analytical setting formulas for Proportional-Integral (PI) state control, this paper applies them to a two-mass oscillator system, commonly used as a simplified model for deep drilling setups. The proposed approach leverages an adaptive algorithm that dynamically tracks the friction torque and adjusts the feedback vector according to the corresponding load input functions. Hereby, the torsional vibrations, induced due to the contact between the drill bit and the rock formation, have been modelled using the static friction (Stribeck) model and measured using different rock samples on a test rig in the form of a scaled-down drilling rig. By integrating these setting formulas with the developed adaptive mechanism, the controller ensures robust performance across a wide range of operating scenarios. Simulation results demonstrate the system's ability to suppress torsional oscillations effectively, achieving significant vibration reduction without compromising the stability of the system. This research extends the theoretical foundations established in prior work and provides a robust framework for advancing vibration control technologies, contributing to safer, more reliable, and efficient operations in the energy industries.

Key words. PI state control, adaptive tracking algorithm, torsional vibrations, nonlinear friction, stick-slip

1. Introduction

In practice, a rotary drilling system is utilised for deep drilling operations in the context of oil and gas production, as well as the exploitation of geothermal fields. This system comprises the top drive, the drill pipe (which can extend up to several kilometres in length), and the lower bottom hole assembly (BHA). The top drive consists of electric motors that transmit the applied torque to the downstream drill string, which in turn transmits it to the drill bit. Due to the nonlinear bit-rock interaction, torsional vibrations will occur during the drilling operation, which can lead to considerable damage to the components of the drill string and the drill bit, reducing the overall efficiency of the system. In [1] it is stated that "approximately one third of system failures have a vibration related root cause" in drilling operations. Among these, the stick-slip phenomenon, which predominantly occurs at low rotational speeds (with frequencies lower than 1 Hz), has a substantial impact on the available torque [1]. As the tribological conditions at the drill bit are nonlinear and depend on numerous, often unknown parameters, the torque at the drill bit is difficult to control. In addition, the exact identification of the current rock layer in which the drill bit is located presents major difficulties, since the data transfer from the drill bit back to the surface can take up to several hours. This makes effective control even more difficult, as the boundary conditions within such a borehole are not available.

The state of the art for the damping of torsional vibrations induced by the stick-slip effect is: 1) reducing the weight on bit (WOB) while simultaneously increasing the rotational speed on the top drive; 2) active damping through using appropriate control. With regard to the first approach, the problem is that reducing the weight on bit leads to a reduced rate of penetration (ROP), while increasing the rotational speed results in unwanted lateral vibrations. For these reasons, the following active vibration damping systems have become established. In [2], the Soft Torque Rotary System (STRS) developed by *Shell* is presented, where the electronic imposition of stiffness by optimizing the speed controller of the top drive and utilising the inertia of the top drive transfers the same resonant frequency for the drill string system to the top drive system. The disadvantage is that the system must be continuously adjusted manually to the current drill string length. The Z-Torque System is presented as an alternative method in [2], which models the drill string as a waveguide and is intended to prevent vibration reflections

on the top drive through active impedance matching. In [3] an optimal control strategy based on dynamic programming (DP) for active damping of stick-slip oscillations was developed. However, such methods have the disadvantage that the direct correlation between the dynamics of the system and the controller parameters is no longer preserved. For this reason, analytical setting formulas for a PI state control have been previously derived in [4], which consider the effect of an increasing negative damping due to nonlinear friction effects on the stability of the open control loop. As a novelty, these formulas are applied in this paper to a two-mass oscillator system and complemented with an innovative developed, adaptive algorithm, which is supposed to be able to dynamically detect the friction torque and adjust the feedback vector depending on the rock formation. The aim is to realize a real-time identification of the existing rock layer, on the basis of which the state controller can effectively dampen torsional vibrations. Another novelty of this paper is the measurement of friction between the drill bit and various rock samples. This is carried out on a specially designed test rig in the form of a scaled-down drilling rig, so that the nonlinear friction effects that occur during deep drilling can be realistically modelled. These measurement results in turn serve as a type of database for the intended real-time identification of the current rock layer within the borehole.

2. Methodology

A. PI state control model

In contrast to the continuous distribution of physical properties such as mass, stiffness or damping over the entire length of the drill string, a reduction of these properties to a finite number of mass points, stiffnesses and dampings is suitable for the control engineering modelling of a deep drilling rig. Lumped-parameter models with two degrees of freedom have been established here, with the top drive representing the first concentrated mass and the drill bit at the end of the drill string representing the second mass.

The PI state control shown in Fig. 1 has been derived for a two-mass oscillator system, characterized by the moment of inertia of the motor J_M and the moment of inertia of the drill bit J_L. The two discrete masses are connected to each other via a spring with the spring stiffness c_{12} and a damper with the damping constant d_{12}. The shaft torque T_{12} therefore acts between the two masses. The air gap torque T_el of the drive machine is defined as the input variable of the controlled system, the output variable corresponds to the drive speed ω_1. The choice of output variable is due to the fact that the drive speed ω_1, in contrast to the load speed ω_2 at the drill bit, can be measured in real time in deep drilling technology. The load side in Fig. 1 is represented via the friction torque T_fric acting on the drill bit, which is modelled by the static friction (Stribeck) model and measured using different rock samples on a test rig (see section 2.).

In the state space representation, the system shown in Fig. 1 is described mathematically using equation (1):

$$\begin{bmatrix} \dot{\boldsymbol{x}}_\mathrm{s} \\ \dot{x}_\mathrm{PI} \end{bmatrix} = \begin{bmatrix} \boldsymbol{A}_\mathrm{s} & \boldsymbol{0} \\ -\boldsymbol{c}_\mathrm{s}^\mathrm{T} & 0 \end{bmatrix} \cdot \begin{bmatrix} \boldsymbol{x}_\mathrm{s} \\ x_\mathrm{PI} \end{bmatrix} + \begin{bmatrix} \boldsymbol{b}_\mathrm{s} \\ 0 \end{bmatrix} \cdot u_\mathrm{s} \qquad (1)$$

It can be seen from equation (1) that the controlled system, which is initially given in the general state space representation, has been extended by a new state variable x_PI. In this way, a PI controller is superimposed on the conventional state controller so that permanent control deviations can be avoided. If this modified controlled system is closed by a state control, the feedback vector $\boldsymbol{r}$ can be calculated according to equation (2):

$$(s-\alpha_1)\dots(s-\alpha_5) = \det\left(s\boldsymbol{I} - (\boldsymbol{A} - \boldsymbol{b}\boldsymbol{r}^\mathrm{T})\right) \qquad (2)$$

The required position of the eigenvalues of the closed loop is specified via the parameters α_1 to α_5, to allow for symbolic solution of the system of equations and to provide analytical setting formulas for the control.

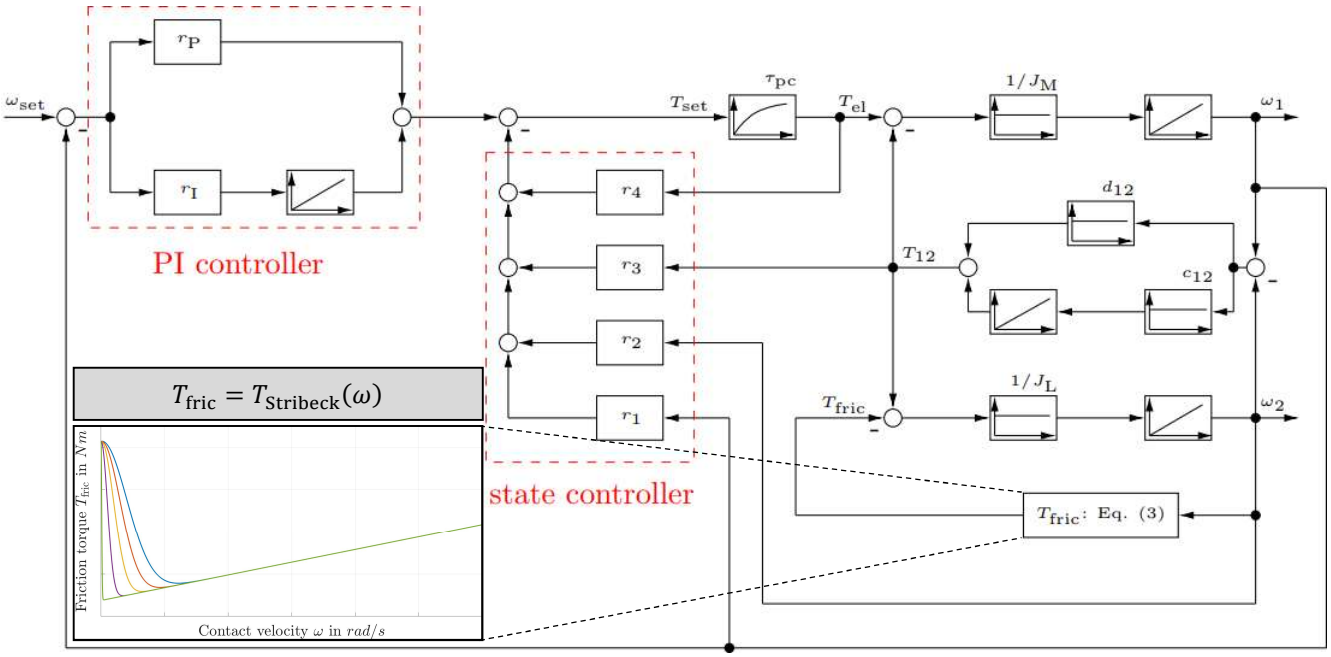

Fig. 1. Control block diagram of the previously developed PI state control of a vibrating drive train in deep drilling technology.

B. Fundamentals of static friction modelling

To calculate the friction torque acting on the drill bit, the static Stribeck model is used, which combines the types of friction that occur - static, dynamic and viscous friction - using the following equation (3) [5]:

$$T_{\mathrm{fric}} = \left(T_{\mathrm{C}} + (T_{\mathrm{S}} - T_{\mathrm{C}}) \cdot e^{-\left|\frac{\omega}{\omega_{\mathrm{S}}}\right|^2} \right) + \sigma_2 \cdot \omega \qquad (3)$$

In this case, the parameter T_{C} is employed to describe the torque in the presence of Coulomb friction, T_{S} is used to denote the static friction torque, ω_{S} signifies the transition from static to dynamic friction, and σ_2 is the viscous friction coefficient. With a usually selected Stribeck shape factor of $\delta_{\mathrm{S}} = 2$, which most accurately simulates the course of the measurement data, the typical shape of the Stribeck curve is shown in Fig. 2.

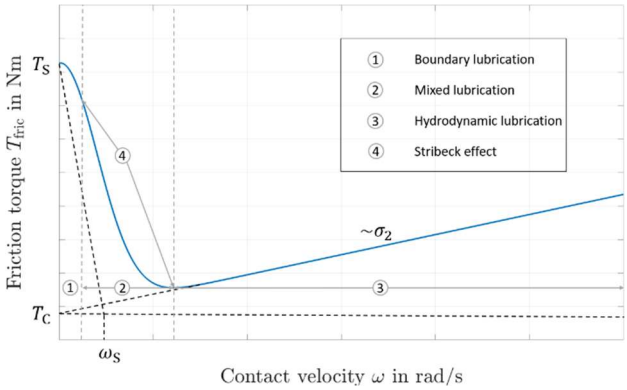

Fig. 2. Typical course of the Stribeck curve, which plots the friction torque T_{fric} as a function of the friction speed ω [5] – [7].

As illustrated in Fig. 2, the Stribeck effect corresponds to a negative damping, or de-attenuation, of the system, characterized by a rapid decrease in the friction torque T_{fric} with increasing speed ω in friction contact. Above a certain speed ω, after the lubrication film is fully formed in the contact region, the friction increases again with increasing speed, which is due to the viscous friction within the lubrication film. This range is largely determined by the lubricant used and, in the case of drilling technology, by the type and quantity of rock excavated. The unknown static friction parameters are then determined using the least squares method, based on a measured data point cloud consisting of N data points according to equation (4):

$$\min_{\mathrm{c}} \| f(\mathrm{c}, x) - y \|_2^2 = \min_{\mathrm{c}} \sum_{i=1}^{N} (f(\mathrm{c}, x_i) - y_i)^2 \qquad (4)$$

In equation (4) x symbolizes the contact velocity ω, y the friction torque T_{fric} and c the unknown friction parameters.

2. Experimental friction measurement and parameter determination

A. Experimental setup and sample preparation

The test setup, designed as a drilling rig and used for friction characterization on various rock samples is shown in Fig. 3.

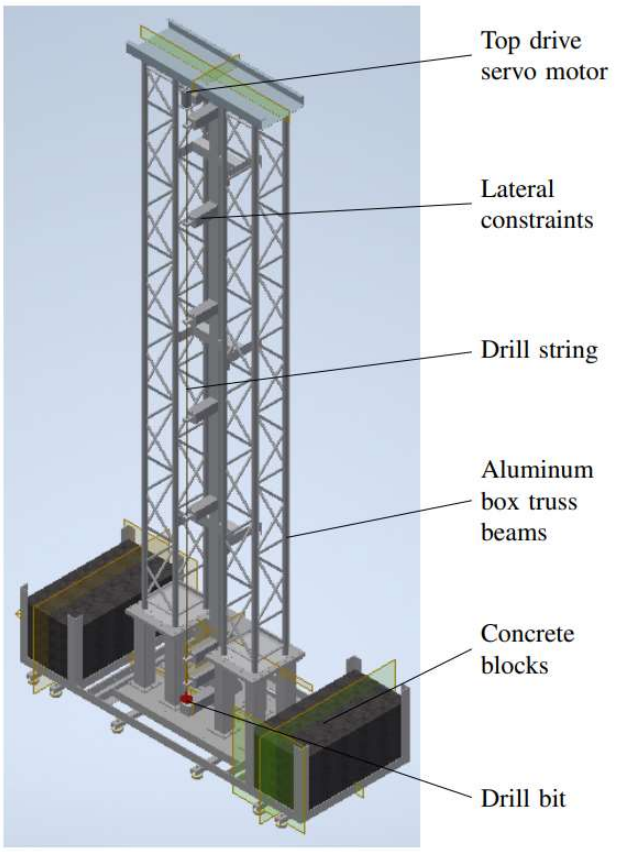

Fig. 3. Experimental setup in the form of a scaled-down drilling rig model (dimensions: H: 5.143 m, L: 1.024 m, D: 1.040 m).

The test rig is operated by a DC motor with an output of 250 W at the top end of the drill string, which is capable of applying a rated torque of 0.8 Nm at a rated current of 6.8 A. A characteristic feature of the test rig is its absence of forward thrust into the rock samples. The corresponding contact pressure of the drill bit on the samples is instead exclusively provided via dead weight of the drill string and a tightening torque of 2.5 Nm applied to the underside of the sample holder. This prevents non-torsional vibrations, such as lateral vibrations caused by bending of the drill pipe due to excessive contact pressure.

The rock samples are pre-drilled with a diamond-coated drill bit on a pillar drill to a depth that allows an identical diamond-coated bit to be clamped onto the test bench and positioned concentrically in the guide (see Fig. 4).

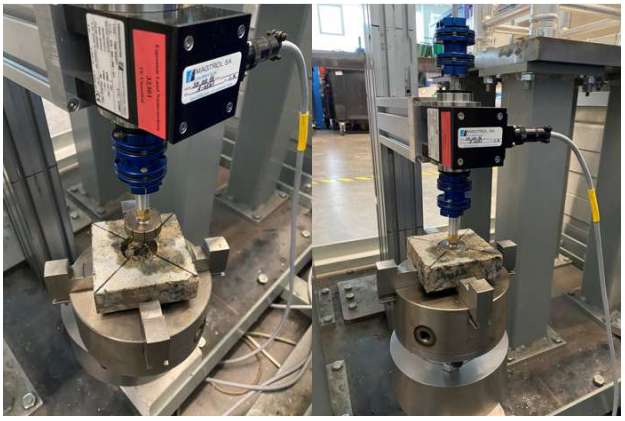

Fig. 4. Setup of the sample holder for clamping the rock samples.

B. Friction model parameter determination

The experiments to characterize the friction and determine the corresponding Stribeck curves were carried out on the test rig shown in Fig. 3 using water as a lubricant for the rock types granite, sandstone and marble. A duration of 20 minutes was scheduled for each set of measurements. The results of the test series in the form of the determined Stribeck curves are shown graphically in Fig. 5.

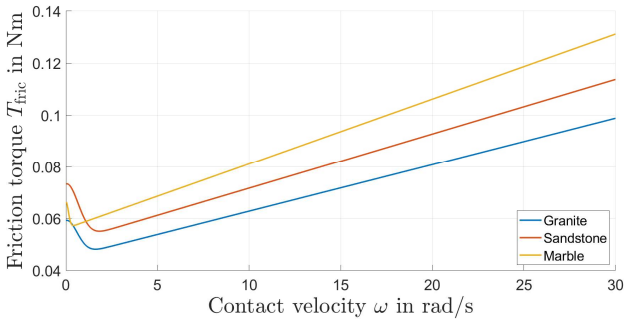

Fig. 5. Comparison of the Stribeck curves measured on the test rig for the three rock samples granite, sandstone and marble.

Fig. 5 shows that the measured friction for the granite sample is lower in direct comparison to the softer rock types sandstone and marble. This becomes particularly clear when looking at the hydrodynamic range, in which the sandstone displays a friction torque that is approximately 10 % higher than that of granite. The reason for this is that the experiment was carried out without any forward thrust into the rock samples. Due to the significantly higher hardness of granite, the weight of the drill string alone or the tightening torque applied below the sample holder does not remove enough material to influence the friction within the lubrication film. The tests for the softer rock types sandstone and marble have shown that, even without a forward thrust, the weight of the drill pipe alone removes significantly more material. The material remaining in the lubrication film causes a substantial increase in friction in the hydrodynamic region of the curve.

Table I lists the static friction parameters determined from the Stribeck curves in Fig. 5. Since the test rig represents a scaled-down drilling rig, the parameters are scaled up by a factor of 500 in the PI state control simulation to highlight friction effects. This factor is derived from the ratio of relevant physical parameters, such as length, diameter, and stiffness, between the real system and the test setup.

Table I. - Static parameters of the Stribeck model, experimentally determined for different rock types.

	Granite	**Sandstone**	**Marble**
T_{C} [Nm]	0.0449	0.0508	0.0562
T_{S} [Nm]	0.0593	0.0734	0.0664
ω_{S} [rad/s]	0.8545	0.9376	0.1917
σ_2 [Nms/rad]	0.0018	0.0021	0.0025

3. Adaptive tracking algorithm

The basis for the development of the adaptive tracking of load input functions is the measurement of Stribeck curves for various rock formations (see Fig. 5). The result is a database which specifies the static friction torque $T_{\mathrm{Stribeck}}(\omega)$ for relevant rocks present in a borehole as a function of the rotational speed of the drill bit ω. To identify the current rock layer, in which the bit is located, the simplified friction torque $T_{\mathrm{fric,calcd.}}$ acting on the drill bit is calculated, see Fig. 6, as stated in equation (5):

$$T_{\mathrm{fric,calcd.}} = T_{\mathrm{driving}} - J_{\mathrm{bit}} \cdot \ddot{\varphi}_{\mathrm{bit}} \tag{5}$$

This calculation, in which T_{driving} represents the driving torque provided by the DC motor (see Fig. 3), J_{bit} the mass inertia of the drill bit and $\ddot{\varphi}_{\mathrm{bit}}$ its angular acceleration, is permissible as long as the friction at the drill bit is the only effective friction in the system. If the difference between the two torques $T_{\mathrm{fric,calcd.}}$ and $T_{\mathrm{Stribeck}}(\omega)$ is within a defined tolerance band with the width ΔT, the corresponding rock layer has been identified by the algorithm. The implementation of a tolerance band appears to be a rational approach, as it serves to mitigate the impact of irregularities in rock structures and potential measurement errors in the characterization of Stribeck curves. For each rock type, the respective feedback vector $\vec{\boldsymbol{r}} = [r_1 \quad r_2 \quad r_3 \quad r_4 \quad r_5]^{\mathrm{T}}$ has been calculated according to the derived analytical setting formulas [4]. This vector is then selected for transfer to a designated holding element in the subsequent step. The holding element, together with the tolerance band ΔT, ensures that the adaptive tracking does not fail even if the calculated torque on the drill bit $T_{\mathrm{fric,calcd.}}$ deviates slightly or temporarily from the measured Stribeck curves $T_{\mathrm{Stribeck}}(\omega)$. As a safety measure in the event that the algorithm is unable to identify a corresponding Stribeck curve, the states are fed back via a previously defined standard feedback vector.

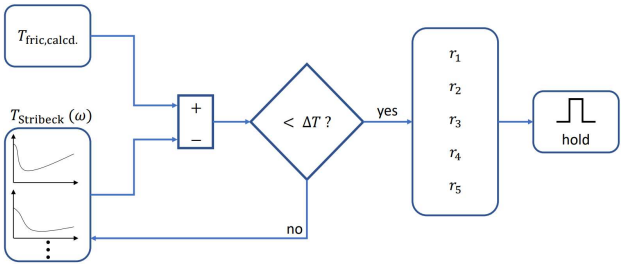

Fig. 6. Flow chart of the adaptive tracking algorithm of the load input function, represented by the measured Stribeck curves.

4. Simulation

A. Boundary conditions of the planned simulation

The simulations were carried out in *Matlab*/*Simulink*, based on the controlled system according to Fig. 1 and the developed adaptive tracking of the load input functions, which are represented by the measured Stribeck curves. An inhomogeneous rock formation was simulated on the load side, in which the rock layers and thus also the Stribeck curves change at certain points in time:

- $t = 10$ s: Starting the top drive in the form of a setpoint jump in the drive speed ω_1 from 0 rad/s to 30 rad/s
- $t = 20$ s: Application of the first load function in the form of a granite rock layer (Fig. 5.: blue curve)
- $t = 30$ s: Application of the second load function in the form of a sandstone rock layer (Fig. 5.: red curve)
- $t = 40$ s: Application of the third load function in the form of a marble rock layer (Fig. 5.: yellow curve)

The mechanical parameters, which are required to populate the system matrix $\boldsymbol{A}_\mathrm{s}$ in equation (1) as well as the selected controller parameters, are listed in the following Table II:

Table II. – Mechanical parameters of a torsion test setup and selected controller parameters T_R and f_R [4].

Parameter	Value	Unit
τ_pc	0.01	s
J_M	1.1348	kgm^2
J_L	1.1348	kgm^2
c_{12}	3.4602	Nm/rad
d_{12}	$1.3189 \cdot 10^4$	Nms/rad
T_R	0.02	–
f_R	0.5	–

Based on the parameters in Table II and the setting formulas from the previous work, the feedback vectors for the analyzed rock samples can be calculated, see Table III.

Table III. – Calculated feedback vectors for the different rocks.

	Granite	Sandstone	Marble
r_1	348.7348	356.7993	391.7814
r_2	−150.7461	−154.1081	−164.1313
r_3	−1.6413	−1.5936	−1.3593
r_4	1.7286	1.7547	1.8629
$-r_5$	$3.5561 \cdot 10^3$	$3.5561 \cdot 10^3$	$3.5561 \cdot 10^3$

B. Simulation results

The result of the simulation is shown in Fig. 7 for the entire length of the simulation period of $t = 50$ s based on the step response of the drive speed ω_1 to a setpoint step at the time $t = 10$ s. The step response clearly shows the influence of the different load functions in the form of the measured Stribeck curves for the rock types granite, sandstone and marble at the times $t = 20$ s, $t = 30$ s and $t = 40$ s. At the time of the load change, the drive speed ω_1 drops due to the sudden load caused by the friction, but is regulated by the PI state controller with a slight overshoot in a short time. To illustrate the behaviour of the developed controller, the load change from the simulated granite formation to sandstone at the time $t = 30$ s is shown enlarged in Fig. 8.

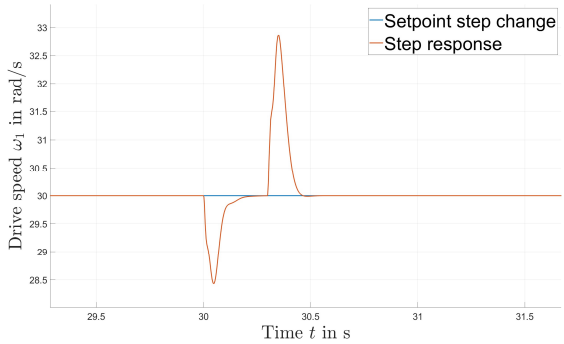

Fig. 8. Enlarged representation of the step response of the drive speed ω_1 during the simulated load change from granite to sandstone at time t=30s.

The enlarged illustration in Fig. 8 shows that the drive speed ω_1 drops to less than 28.5 rad/s during the load change due to the increased friction. However, the PI state control is able to completely dampen the induced vibration after around 500 ms. In addition, it can be seen that at time $t = 30.3$ s there is an overshoot in the drive speed ω_1 up to approximately 33 rad/s. This is related to the feedback vectors assigned by the adaptive algorithm, which are shown in the following Fig. 9.

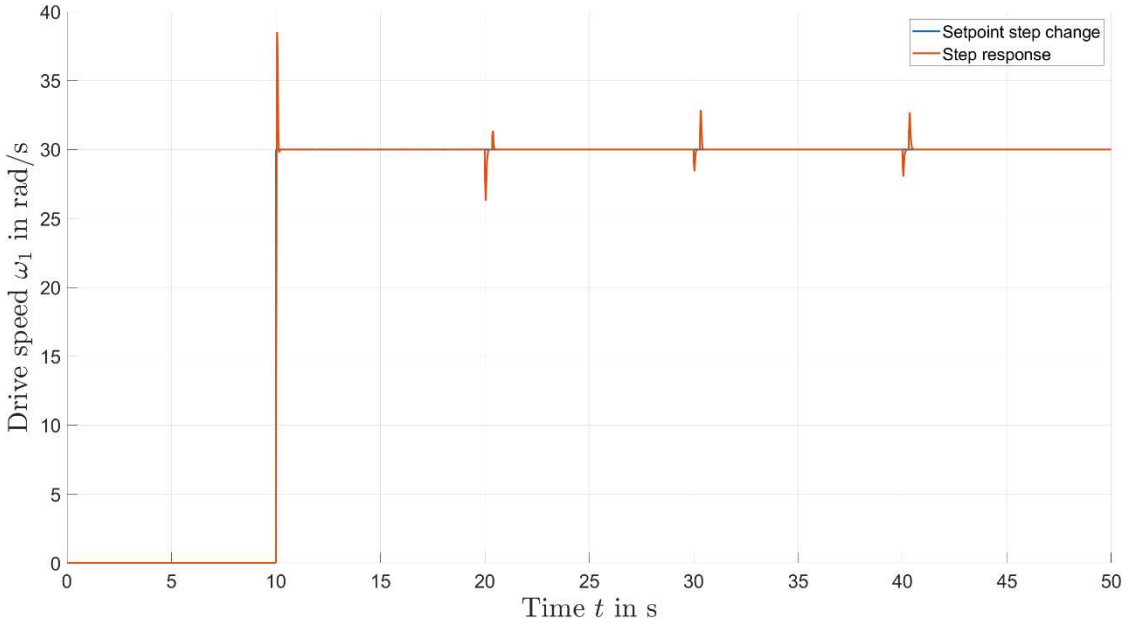

Fig. 7. Display of the simulated step response of the drive speed ω_1 after a defined setpoint step change at the time $t = 10$ s.

a) First feedback vector assigned by the adaptive algorithm.

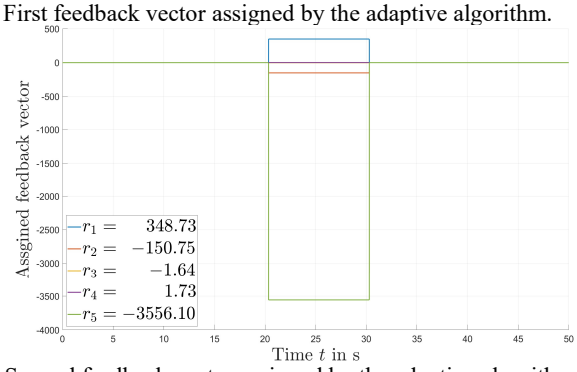

b) Second feedback vector assigned by the adaptive algorithm.

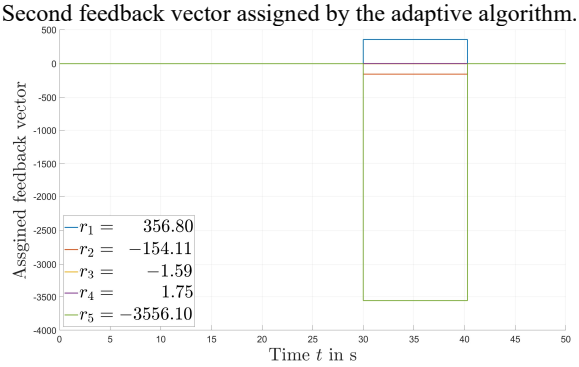

c) Third feedback vector assigned by the adaptive algorithm.

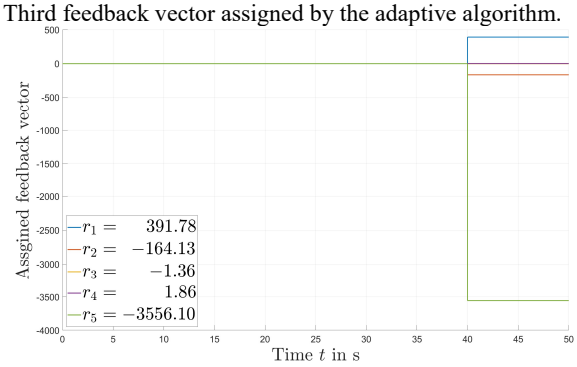

Fig. 9. Representation of the feedback vectors assigned by the adaptive algorithm in the simulation period of $t = 50$ s.

Fig. 9, a) to c), provides several insights into the controller behavior and the developed adaptive tracking of load input functions. On the one hand, it can be seen that the adaptive algorithm is able to recognize the areas of the various applied loads. Fig. 9 a) shows the feedback vector first assigned by the algorithm over a period of approximately $t = 20$ s to around $t = 30$ s. For the period $t = 30$ s to roughly $t = 40$ s, the algorithm assigns the next feedback vector (see Fig. 9 b)). The last feedback vector is then assigned at time $t = 40$ s until the end of the simulation (see Fig. 9 c)). On the other hand, the comparison of the assigned feedback vectors with the feedback vectors calculated according to Table III reveals that not only the time ranges of the different load input functions are correctly recognized by the algorithm, but also the corresponding feedback vectors are accurately assigned to the respective rock type. Lastly, it can be stated that the periods of the respective effective friction torques are generally detected correctly, but due to the implemented holding element, these ranges are sometimes exceeded for a short period of time (see Fig. 9, a) and b)). This means that both the current and previous feedback vector are temporarily effective, leading to the overshoot in the step response (see Fig. 7 and 8). This occurs after the disappearance of the previous feedback vector.

5. Conclusion

Torsional vibrations in drilling operations substantially reduce the efficiency of the system and cause serious damage to the drive shaft components. In contrast to numerical controller design methods, in which the direct correlation between the dynamics and the controller parameters is lost, the previously derived PI state controller demonstrates significant advantages in mitigating torsional vibrations in combination with the adaptive tracking algorithm, developed in this paper. Such vibrations can be successfully damped by this approach while still maintaining access to the damping behaviour of the system through the controller parameters. The adaptive tracking also enables robust control behaviour in the event of inaccuracies in the friction measurement. However, the presented method has certain limitations as it assumes accurate modelling of the system and relies on precise parameter identification. In addition, the implementation of a state observer may be required to estimate system states in real time, especially in cases where direct measurements are not feasible. Beyond drilling, the framework may be adapted to other mechanical systems involving torsional dynamics, such as wind turbine drivetrains. When applying this control and the adaptive algorithm to other systems, it is important to ensure that the mechanical parameters are adapted to the new conditions and that the corresponding feedback vectors are recalculated with regard to the effective load functions.

Acknowledgement

Funded by the Deutsche Forschungsgemeinschaft (DFG, German Research Foundation) – 512815763.

References

[1] A. Hohl et al., “The Nature of the Interaction Between Stick/Slip and High-Frequency Torsional Oscillations”, IADC/SPE International Drilling Conference and Exhibition SPE-199642-MS (2020)., pp. 2.

[2] S. Dwars, “Recent Advances in Soft Torque Rotary Systems”, SPE/IADC Drilling Conference and Exhibition SPE/IADC-173037-MS (2015)., pp. 1.

[3] T. Feng, H. Zhang and D. Chen, “Dynamic Programming Based Controllers to Suppress Stick-Slip in A Drilling System”, American Control Conference (2017)., pp. 1.

[4] D. Piontek et al., “Derivation of analytical setting formulas for PI control of electrical drives for active torque damping in deep drilling technology”, International Symposium on Power Electronics, Electrical Drives, Automation and Motion (SPEEDAM) (2024)., pp. 1.

[5] J. M. C. de Sousa, “Analyse der Ursachen des Stick-Slip-Effekts an Bahnenerzeugnissen für die Anwendung im Fahrzeuginnenraum am Beispiel von PVC,” Ph.D. dissertation, Institute of Ceramics, Refractories and Composites, Freiberg University, Freiberg, Germany, 2007.

[6] A. Kramer, and J. Kempkes, “Modellierung und Simulation von nichtlinearen Reibungseffekten bei der Lageregelung von Servomotoren,” in FHWS SCIENCE JOURNAL, vol. 1, 2013, p. 50.

[7] M. Wirth, “Schleppmomente in Synchronisierungen von Fahrzeuggetrieben,” Ph.D. dissertation, Institute of Mechanical and Vehicle Engineering, Technical University of Munich, Munich, Germany, 2012.